

## DETERMINATION OF ACTIVATION ENERGY FOR GRAIN GROWTH OF ELECTROSPUN $ZnFe_2O_4$ NANOFIBERS

Van Hoang Nguyen<sup>1,\*</sup>, Minh Duc Le<sup>1</sup>, Manh Hung Nguyen<sup>1</sup>,  
Van Duy Nguyen<sup>2</sup>, Duc Hoa Nguyen<sup>2</sup>, Van Hieu Nguyen<sup>3</sup>

<sup>1</sup>*Le Quy Don Technical University, Hanoi, Vietnam*

<sup>2</sup>*Hanoi University of Science and Technology, Hanoi, Vietnam*

<sup>3</sup>*Phenikaa University, Hanoi, Vietnam*

### Abstract

In this study,  $ZnFe_2O_4$  nanofibers were fabricated by facile electrospinning method and subsequent calcination process. The scanning electron microscopy (SEM) images showed that  $ZnFe_2O_4$  nanofibers which were in diameters of 30-100 nm and consisted of nanograins had typical morphologies of spider nets. The X-ray diffraction (XRD) patterns revealed the typical cubic structure of the  $ZnFe_2O_4$  nanofibers. The energy dispersive X-ray spectroscopy (EDX) results exhibited the presence of Zn, Fe, and O elements in the synthesized nanofibers. The results indicated that the nanograins size increased with the increase of annealing temperatures. The activation energy for grain growth in electrospun  $ZnFe_2O_4$  nanofibers was estimated to be 10 kJ/mol. Since this value of activation energy was quite small, nanograins easily grew during the calcination process.

**Keywords:** *Activation energy;  $ZnFe_2O_4$ ; nanofibers; electrospinning.*

### 1. Introduction

Nanofibers (NFs) are 1D nanostructures which are increasingly used in many fields like water treatment [1, 2], photocatalysis [1, 3], batteries [4], magnetics [5], supercapacitors [6], and gas sensors [7-9] because of their outstanding properties including porous structure, large surface area-to-volume ratio and flexible surface functionalities [1, 2]. Different approaches have been reported for the synthesis of NFs such as drawing, template synthesis, phase separation, self-assembly, and electrospinning [1, 2]. Among them, electrospinning appears to be the most versatile, low-cost method to fabricate NFs.

Oxide NFs prepared by the electrospinning method consist of nanograins which form during heat treatment process. Nanograin sizes significantly influence the physical and chemical properties of oxide nanofibers. Nanograins grow with increased annealing

---

\* Email: hoangmse@lqdtu.edu.vn

temperature and annealing time [10, 11]. Generally, the grain growth occurs in polycrystalline materials to reduce the free energy of the system caused by the decrease in the total grain boundary energy. The grains grow because atoms (or ions) diffuse more readily from the convex surface on one side of the grain boundary to the concave surface on the other side than in the opposite direction [12]. The net flow from the convex to the concave side is due to the fact that the chemical potential of the atoms on the convex surface is higher than that of the atoms on the concave surface [12]. This net flow causes the boundary to move toward its center of curvature, which results in the grain growth. Therefore, the growth of nanograins can be roughly regarded as a thermally activated diffusion process that satisfies the well-known Arrhenius equation [13-15]:

$$D = A.e^{\frac{-E_a}{RT}} \quad (1)$$

where  $D$  is the average grain size (nm),  $A$  is a constant referred to as the pre-exponential factor,  $E_a$  is the activation energy for the grain growth ( $\text{J.mol}^{-1}$ ),  $R$  is the gas constant ( $R = 8.314 \text{ J.mol}^{-1}.\text{K}^{-1}$ ), and  $T$  is the absolute temperature (K).

The activation energy,  $E_a$ , of the grain growth can be calculated by transforming (1) into its logarithmic form:

$$\ln D = \ln A - \frac{E_a}{RT} \quad (2)$$

Thus,  $E_a$  can be determined by the slope of  $\ln(D)$  against  $T^{-1}$ . The study of the activation energy brings benefits to the control of the grain size to achieve the desired properties. Therefore, determination of the activation energy for the grain growth of electrospun oxide NFs has attracted tremendous interest. Accordingly, the activation energy of various oxide NFs, including  $\text{SnO}_2$  [16],  $\text{ZnO}$  [13],  $\text{NiO}$  [14],  $\text{CuO}$  [17], and  $\text{Co}_3\text{O}_4$  [18], has been thoroughly investigated. The activation energy for the grain growth for other structure types of  $\text{ZnFe}_2\text{O}_4$  like nanoparticles [19, 20] or sintered nanopowders [21] has also been surveyed; however, up to present, there have been no reports on the activation energy for the grain growth of electrospun  $\text{ZnFe}_2\text{O}_4$  NFs which have exhibited as a promising ternary semiconductor oxide for many applications such as gas sensors [10], batteries [22, 23], and supercapacitors [6, 24].

In this study,  $\text{ZnFe}_2\text{O}_4$  NFs were prepared by electrospinning method. Characterizations of synthesized NFs were carefully investigated and the growth behavior of nanograins in individual electrospun  $\text{ZnFe}_2\text{O}_4$  NFs was studied. The activation energy for grain growth of nanograins in the NFs was also calculated.

## 2. Experiments

### 2.1. $ZnFe_2O_4$ NFs preparation

$Fe(NO_3)_3 \cdot 9H_2O$  (Xilong Chemical Co.) and  $Zn(CH_3COO)_2 \cdot 2H_2O$  (Merck Co.) were used as precursor salts. PVA ( $M_w \approx 130.000$  Da) was supplied from the Sigma-Aldrich. All chemical reagents were used in AR grade without further purification.

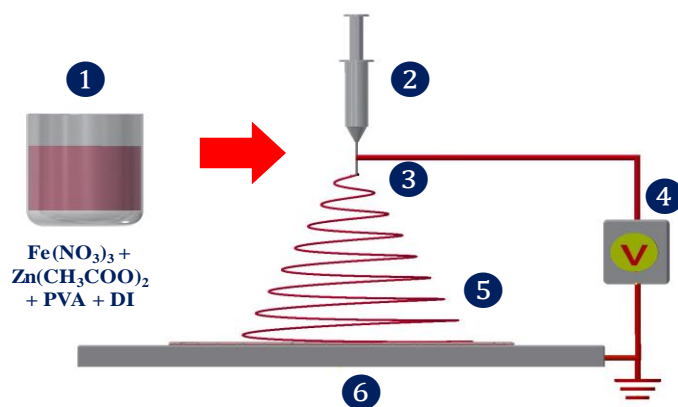


Fig. 1. Schematic diagram of  $ZnFe_2O_4$  NFs prepared by electrospinning: 1- precursor solution, 2- syringe, 3- needle, 4- DC high voltage power supply, 5- as-spun nanofibers, 6- collector

NFs formation makes use of electrostatic forces to stretch a viscoelastic solution. Schematic illustration of NFs synthesis by typical electrospinning method is shown in Fig. 1 as reported in our previous works [10, 11]. First, a certain amount of  $Fe(NO_3)_3$ ,  $Zn(CH_3COO)_2$  (2:1 molar ratio of Fe:Zn) and PVA were completely dissolved in DI with a magnetic stirrer to obtain a homogeneous brown-red solution. The electrospinning process began when a high DC voltage was applied to the needle while the metal collector was grounded. Under the influence of the electrostatic field, the spherical droplet was deformed into a Taylor cone. When the voltage surpassed a critical value, the charged liquid jet emerged from the cone. The internal and external charge forces caused the whipping of the liquid jet in the direction of the collector and formed a continuous and thin fiber on the surface of the collector [25, 26]. The mixture solution was electrospun for 3 h. The as-spun fibers were then calcined at the annealing temperature from 400 to 700°C for 3 h in air to form  $ZnFe_2O_4$  NFs.

### 2.2. Characterization

The thermogravimetric analysis (TGA) and derivative thermogravimetric (DTG) were used to determine the annealing temperature of the as-spun fibers. The analysis was carried out on a Netzsch STA 409 PC thermal analyzer with a heating rate of 10°C/min. The morphology and microstructure of NFs were examined by field-emission

electron microscopy (FESEM Hitachi S-4800). The crystal structure was characterized by X-ray diffraction (XRD) using a D5005 diffractometer Bruker with Cu K $\alpha$  radiation ( $\lambda = 0.154056$  nm). Phase identification was carried out by comparison with the registered pattern of Joint Committee on Powder Diffraction Standards (JCPDS). Nanograin size was calculated from the most intense peak, corresponding to (311) reflection by using the Scherrer formula [19, 27]:

$$D = 0.9\lambda / (\beta \cos \theta) \quad (3)$$

in which  $\lambda$  is the X-ray wavelength,  $\theta$  is the diffraction angle of the (311) planes of ZnFe<sub>2</sub>O<sub>4</sub> NFs and  $\beta$  is the full width at half maximum (FWHM) of the observed peak. The element analysis was performed by energy dispersive X-ray spectroscopy (EDX, attached to FESEM Hitachi S-4800).

### 3. Results and discussion

The TGA, DTG results and FESEM image of the as-spun fibers are shown in Fig. 2. According to the result of TGA-DTG in Fig. 2a, the minor weight loss below 150°C was caused by the evaporation of residual and absorbed water in the as-spun fibers [28] while the major weight loss in the temperature range of 200-300°C was attributed to the decomposition of zinc acetate, ferrite nitrate and dehydration on the polymer side chain [28, 29]. A further weight loss in TGA between 300 and 450°C was related to the pyrolysis of the main chain of the polymer and the continuous decomposition of zinc acetate and ferrite nitrate to form crystalline ZnFe<sub>2</sub>O<sub>4</sub> [28-30]. However, almost no change in weight loss above 500°C was detected, indicating that the decomposition of the as-spun fibers had completed. As shown in Fig. 2b, as-spun ZnFe<sub>2</sub>O<sub>4</sub> fibers with the average diameter of about 200-400 nm were like a spider net which is typical electrospun NFs morphology as reported in many works [13, 14, 16-18]. The fibers were also uniform, continuous and well-dispersed.

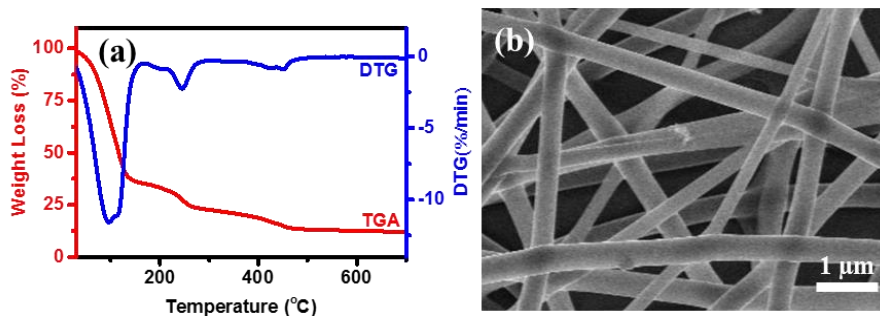


Fig. 2. (a) TGA and DTG curves for decomposition and (b) FE-SEM image of as-spun fibers

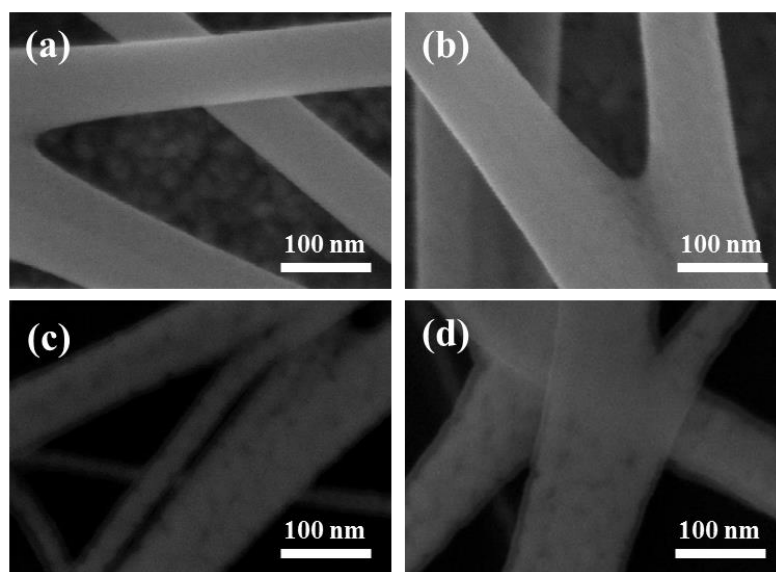


Fig. 3. FE-SEM images of  $ZnFe_2O_4$  NFs calcined at (a) 400, (b) 500, (c) 600 and (d) 700°C

Fig. 3 shows FESEM images obtained from  $ZnFe_2O_4$  NFs after calcination at different annealing temperatures from 400 to 700°C for 3 h in air. It can be seen that the fibers diameters shrank to 30-100 nm because of the evaporation of water, the pyrolysis of the PVA and the decomposition of metal salts in the as-spun fibers during

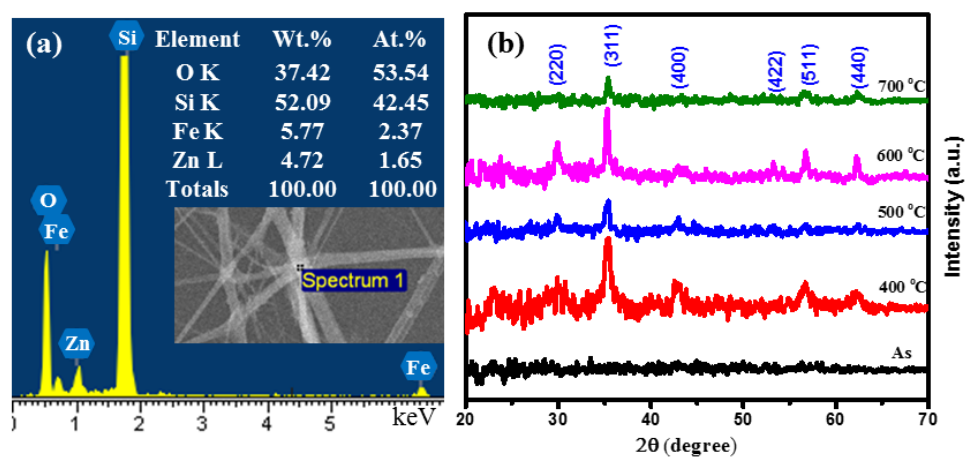


Fig. 4. EDX spectrum (a) of  $ZnFe_2O_4$  NFs calcined at 600°C and XRD patterns (b) of as-spun fibers and  $ZnFe_2O_4$  NFs calcined at different annealing temperatures from 400 to 700°C for 3 h in air

calcination. However, the continuous structure of the  $ZnFe_2O_4$  NFs was retained, and the morphology of the as-spun fibers was undamaged. The NFs surface became rougher because of comprising many nanograins. The higher the annealing temperature was the rougher NFs surface became due to the nanograin growth. It can be explained by the fact that the nanograins in individual NFs were not in a thermodynamic equilibrium state. When annealing temperature increased, the nanograins tended to undergo a growth process by substantially reducing the grain boundaries, leading to a reduction in the number of nanograins and an increase in nanograin size, then resulting in reducing the surface free energy [12].

Table 1. Average nanograin sizes determined by Scherrer formula of (311) diffraction peak of  $ZnFe_2O_4$  NFs calcinated at annealing temperatures from 400 to 700°C.

Anneal. Temp. (°C)	1000/T (1/K)	Nanograin size, D (nm)		ln (D) (nm)	
		This work	Ref. [10] data	This work	Ref. [10] data
400	1.49	11.6	13.5	2.45	2.60
500	1.29	14	14.9	2.64	2.70
600	1.15	17.2	18	2.84	2.89
700	1.03	19.7	23.9	2.98	3.17

The chemical compositions of  $ZnFe_2O_4$  NFs are shown in EDX result (Fig. 4a). The result revealed the presence of Zn, Fe, and O elements in  $ZnFe_2O_4$  NFs. The presence of Si element came from the Si/SiO<sub>2</sub> substrate. The cubic spinel structure of  $ZnFe_2O_4$  NFs at different annealing temperatures was also confirmed in XRD pattern (Fig. 4b). Clearly, as-spun fibers displayed no diffraction peaks due to their amorphous status while the calcined samples revealed that all the peaks of (220), (311), (400), (422), (511) and (440) agreed well with standard value of JCPDS card No. 89–7412 for the cubic spinel structure of  $ZnFe_2O_4$ . This confirmed the formation of pure  $ZnFe_2O_4$  phase after calcination at annealing temperatures. Average grain sizes of  $ZnFe_2O_4$  NFs calculated from the experimental XRD data using (3) are exhibited in Tab. 1 which shows that nanograins increased from 11.6 to 19.7 nm with the increase of annealing temperature from 400 to 700°C. This result agreed well with trend of grain growth with increased annealing temperature from above-mentioned FESEM images.

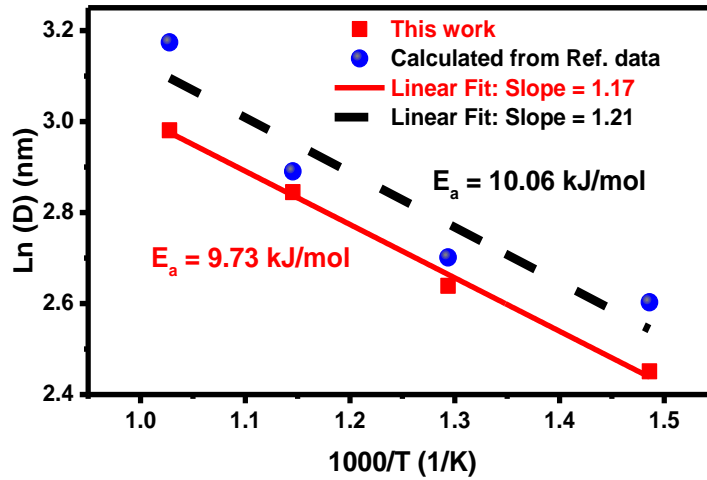


Fig. 5. Plot of  $\ln(D)$  versus  $1/T$ . The slope gives the information about the activation energy for grain growth

The growth behavior of nanograins in  $\text{ZnFe}_2\text{O}_4$  NFs at various annealing temperatures from 400 to 700°C was also investigated. The nanograin growth in the NFs at high annealing temperature was driven by obtaining a minimum free energy caused by reduction of total grain boundary energy. Atoms from one nanograin underwent dissolution and were then transferred to another nanograin. This resulted in a net atomic diffusion from the nanograins with a smaller size to larger nanograins, leading to the growth of the nanograins in the NFs [17]. Fig. 5 illustrates the plot of  $\ln(D)$  as a function of  $1/T$  from data in the Tab. 1.  $E_a$  was estimated to be about 9.73 kJ/mol from the slope of linear fit, which was nearly the same as the value of 10.06 kJ/mol obtained by calculating from the nanograin size data of  $\text{ZnFe}_2\text{O}_4$  NFs in Ref. [10]. Tab. 2 shows the comparison of activation energy of  $\text{ZnFe}_2\text{O}_4$  NFs to that of other nanostructures. The activation energy of NFs obtained in the present study was quite close to that of nanoparticles and much lower than that of sintered powders. It is due to the fact that nanograins in electrospun NFs had chemical potential higher than that of larger grains, resulting in their lower activation energy and being more active in growth [17]. According to Katoch et al. [12], the chemical potential of atoms in nanoscale grains became higher because of the increase of the grain boundary area; thus, the atoms in nanograins participated more actively in the grain growth. Therefore, nanograins possessed the chemical potential higher than that of larger grains, which consequently led to their lower activation energy because nanograins were likely to grow promptly during calcination process.

Table 2. The comparison of activation energy for grain growth

ZnFe <sub>2</sub> O <sub>4</sub> structures	Preparation method	Nanograin size (nm)	Annealing temperatures (°C)	Act. Energy $E_a$ (kJ/mol)	Ref.
Nanoparticle	Coprecipitation	10 – 27	600 – 1000	18.2	[19]
Nanoparticle	Mechanochemical	19 – 35	550 – 800	18.5	[20]
Sintered nanopowder	Mechanochemical	48.12	1100	38.11	[21]
NFs	Electrospinning	11.6 – 19.7	400 – 700	9.73	This work
		13.5 – 23.9		10.06	

#### 4. Conclusion

ZnFe<sub>2</sub>O<sub>4</sub> NFs were successfully fabricated by electrospinning method. ZnFe<sub>2</sub>O<sub>4</sub> NFs had a diameter of 30-100 nm and consisted of many nanograins. The nanograin size increased from 11.6 to 19.7 nm with the increase of annealing temperatures between 400 and 700°C. Higher annealing temperatures resulted in the growth of nanograins in the individual NFs for reducing the grain boundaries area. The activation energy for the growth of nanograins was estimated to be about 10 kJ/mol. This small value of activation energy made the grain growth inhibition be weaker; as a result, the nanograins grew easily during calcination process.

#### Acknowledgement

This work was supported by the regular research projects 2020-2021 (Le Quy Don Technical University) under grant number 20.1.014 (3859/QĐ-HV).

#### References

- [1] Panthi, G., Park, M., Kim, H. Y., Lee, S. Y., & Park, S. J., "Electrospun ZnO hybrid nanofibers for photodegradation of wastewater containing organic dyes: A review," *Journal of Industrial and Engineering Chemistry*, 21, 26-35, 2015. <https://doi.org/10.1016/j.jiec.2014.03.044>
- [2] Halim, N. S. A., Wirzal, M. D. H., Hizam, S. M., Bilad, M. R., Nordin, N. A. H. M., Sambudi, N. S., ... Yusoff, A. R. M., "Recent Development on Electrospun Nanofiber Membrane for Produced Water Treatment: A review," *Journal of Environmental Chemical Engineering*, 9(1), 104613-104633, 2021. <https://doi.org/10.1016/j.jece.2020.104613>
- [3] Jo, S., Kim, H., & Lee, T. S., "Decoration of conjugated polyquinoxaline dots on mesoporous TiO<sub>2</sub> nanofibers for visible-light-driven photocatalysis," *Polymer*, 228, 123892–123903, 2021. <https://doi.org/10.1016/j.polymer.2021.123892>

- [4] Wen, J., Pei, Y., Liu, L., Su, D., Yang, M., Wang, Q., ... Wang, X., "Fully encapsulated  $\text{Sb}_2\text{Se}_3/\text{Sb}/\text{C}$  nanofibers: Towards high-rate, ultralong-lifespan lithium-ion batteries," *Journal of Alloys and Compounds*, 874, 159961, 2021. <https://doi.org/10.1016/j.jallcom.2021.159961>
- [5] Hu, Q., Yue, B., Yang, F., Shao, H., Bao, M., Wang, Y., & Liu, J., "Electrochemical and magnetic properties of perovskite type  $\text{RMnO}_3$  (R = La, Nd, Sm, Eu) nanofibers," *Journal of Alloys and Compounds*, 872, 159727, 2021. <https://doi.org/10.1016/j.jallcom.2021.159727>
- [6] Yang, S., Ai, J., Han, Z., Zhang, L., Zhao, D., Wang, J.,... Cao, B., "Electrospun  $\text{ZnFe}_2\text{O}_4$ /carbon nanofibers as high-rate supercapacitor electrodes," *Journal of Power Sources*, 469, 228416-228423, 2020. <https://doi.org/10.1016/j.jpowsour.2020.228416>
- [7] Morais, P. V., Suman, P. H., Silva, R. A., & Orlandi, M. O., "High gas sensor performance of  $\text{WO}_3$  nanofibers prepared by electrospinning," *Journal of Alloys and Compounds*, 864(2), 158745, 2021. <https://doi.org/10.1016/j.jallcom.2021.158745>
- [8] Phuoc, P. H., Hung, C. M., Van Toan, N., Van Duy, N., Hoa, N. D., & Van Hieu, N., "One-step fabrication of  $\text{SnO}_2$  porous nanofiber gas sensors for sub-ppm  $\text{H}_2\text{S}$  detection," *Sensors and Actuators, A: Physical*, 303, 111722-111734, 2020. <https://doi.org/10.1016/j.sna.2019.111722>
- [9] Hung, C. M., Phuong, H. V., Van Thinh, V., Hong, L. T., Thang, N. T., Hanh, N. H., ... Hoa, N. D., "Au doped  $\text{ZnO}/\text{SnO}_2$  composite nanofibers for enhanced  $\text{H}_2\text{S}$  gas sensing performance," *Sensors and Actuators, A: Physical*, 317, 112454-112456, 2021. <https://doi.org/10.1016/j.sna.2020.112454>
- [10] Van Hoang, N., Hung, C. M., Hoa, N. D., Van Duy, N., & Van Hieu, N., "Facile on-chip electrospinning of  $\text{ZnFe}_2\text{O}_4$  nanofiber sensors with excellent sensing performance to  $\text{H}_2\text{S}$  down ppb level," *Journal of Hazardous Materials*, 360(May), 6-16, 2018. <https://doi.org/10.1016/j.jhazmat.2018.07.084>
- [11] Van Hoang, N., Hung, C. M., Hoa, N. D., Van Duy, N., Van Toan, N., Hong, H. S.,... Van Hieu, N., "Enhanced  $\text{H}_2\text{S}$  gas-sensing performance of  $\alpha\text{-Fe}_2\text{O}_3$  nanofibers by optimizing process conditions and loading with reduced graphene oxide," *Journal of Alloys and Compounds*, 826, 2020. <https://doi.org/10.1016/j.jallcom.2020.154169>
- [12] Katoch, A., Choi, S. W., & Kim, S. S., "Nanograins in electrospun oxide nanofibers," *Metals and Materials International*, 21(2), 213-221, 2015. <https://doi.org/10.1007/s12540-015-4319-8>
- [13] Park, J. Y., & Kim, S. S., "Growth of nanograins in electrospun  $\text{ZnO}$  nanofibers," *Journal of the American Ceramic Society*, 92(8), 1691-1694, 2009. <https://doi.org/10.1111/j.1551-2916.2009.03119.x>
- [14] Choi, S. W., Park, J. Y., & Kim, S. S., "Growth behavior of nanograins in  $\text{NiO}$  fibers," *Materials Chemistry and Physics*, 127(1-2), 16-20, 2011. <https://doi.org/10.1016/j.matchemphys.2011.01.049>
- [15] Aminirastabi, H., Xue, H., Mitić, V. V., Lazović, G., Ji, G., & Peng, D., "Novel fractal analysis of nanograin growth in  $\text{BaTiO}_3$  thin film," *Materials Chemistry and Physics*, 239, 122261-122271, 2020. <https://doi.org/10.1016/j.matchemphys.2019.122261>

- [16] Park, J. Y., Asokan, K., Choi, S. W., & Kim, S. S., "Growth kinetics of nanograins in SnO<sub>2</sub> fibers and size dependent sensing properties," *Sensors and Actuators, B: Chemical*, 152(2), 254–260, 2011. <https://doi.org/10.1016/j.snb.2010.12.017>
- [17] Choi, S. W., Park, J. Y., & Kim, S. S., "Growth behavior and sensing properties of nanograins in CuO nanofibers," *Chemical Engineering Journal*, 172(1), 550–556, 2011. <https://doi.org/10.1016/j.cej.2011.05.100>
- [18] Choi, S. W., Park, J. Y., & Kim, S. S. Growth kinetics of nanograins in Co<sub>3</sub>O<sub>4</sub> fibers. *Ceramics International*, 37(1), 427–430, 2011. <https://doi.org/10.1016/j.ceramint.2010.09.002>
- [19] Philip, J., Gnanaprakash, G., Panneerselvam, G., Antony, M. P., Jayakumar, T., & Raj, B., "Effect of thermal annealing under vacuum on the crystal structure, size, and magnetic properties of ZnFe<sub>2</sub>O<sub>4</sub> nanoparticles," *Journal of Applied Physics*, 102(5), 1-7, 2007. <https://doi.org/10.1063/1.2777168>
- [20] Yang, H., Zhang, X., Huang, C., Yang, W., & Qiu, G., "Synthesis of ZnFe<sub>2</sub>O<sub>4</sub> nanocrystallites by mechanochemical reaction." *Journal of Physics and Chemistry of Solids*, 65(7), 1329-1332, 2004. <https://doi.org/10.1016/j.jpcs.2004.03.001>
- [21] Lazarević, Z. Ž., Jovalekić, Č., Milutinović, A., Sekulić, D., Ivanovski, V. N., Rečnik, A., ... Ž. Romčević, N., "Nanodimensional spinel NiFe<sub>2</sub>O<sub>4</sub> and ZnFe<sub>2</sub>O<sub>4</sub> ferrites prepared by soft mechanochemical synthesis," *Journal of Applied Physics*, 113(18), 0-11, 2013. <https://doi.org/10.1063/1.4801962>
- [22] Gao, Y., Yin, L., Kim, S. J., Yang, H., Jeon, I., Kim, J. P., ... Cho, C. R., "Enhanced lithium storage by ZnFe<sub>2</sub>O<sub>4</sub> nanofibers as anode materials for lithium-ion battery," *Electrochimica Acta*, 296, 565-574, 2019. <https://doi.org/10.1016/j.electacta.2018.11.093>
- [23] Chem, J. M., Teh, P. F., Sharma, Y., Pramana, S., & Srinivasan, M., "Nanoweb anodes composed of one-dimensional, high aspect ratio, size tunable electrospun ZnFe<sub>2</sub>O<sub>4</sub> nanofibers for lithium ion batteries," *Journal of Materials Chemistry*, 21(38), 14999-15008, 2011. <https://doi.org/10.1039/c1jm12088c>
- [24] Agyemang, F. O., & Kim, H., "Electrospun ZnFe<sub>2</sub>O<sub>4</sub>-based nanofiber composites with enhanced supercapacitive properties," *Materials Science and Engineering B*, 211, 141-148, 2016. <https://doi.org/10.1016/j.mseb.2016.06.011>
- [25] Schiffman, J. D., & Schauer, C. L., "A Review: Electrospinning of Biopolymer Nanofibers and their Applications," *Polymer Reviews*, 48(2), 317-352, 2008. <https://doi.org/10.1080/15583720802022182>
- [26] Haider, A., Haider, S., & Kang, I.-K., "A comprehensive review summarizing the effect of electrospinning parameters and potential applications of nanofibers in biomedical and biotechnology," *Arabian Journal of Chemistry*, 11(8), 1165-1188, 2018. <https://doi.org/10.1016/j.arabjc.2015.11.015>
- [27] Cullity, B. D., & Stock, S. R., *Elements of X-Ray Diffraction: Pearson*. Pearson, 2014.
- [28] Zhang, G., Li, C., Cheng, F., & Chen, J., "ZnFe<sub>2</sub>O<sub>4</sub> tubes: Synthesis and application to gas sensors with high sensitivity and low-energy consumption," *Sensors and Actuators, B: Chemical*, 120(2), 403-410, 2007. <https://doi.org/10.1016/j.snb.2006.02.034>

- [29] Arias, M., Pantojas, V. M., Perales, O., & Otaño, W., "Synthesis and characterization of magnetic diphasic ZnFe<sub>2</sub>O<sub>4</sub>/γ-Fe<sub>2</sub>O<sub>3</sub> electrospun fibers," *Journal of magnetism and magnetic materials*, 323(16), 2109-2114, 2011. <https://doi.org/10.1016/j.jmmm.2011.02.018>
- [30] Yang, J. M., & Yen, F. S., "Evolution of intermediate phases in the synthesis of zinc ferrite nanopowders prepared by the tartrate precursor method," *Journal of Alloys and Compounds*, 450(1-2), 387-394, 2008. <https://doi.org/10.1016/j.jallcom.2006.10.139>

## XÁC ĐỊNH HOẠT NĂNG TRONG QUÁ TRÌNH PHÁT TRIỂN HẠT CỦA SỢI NANO ZnFe<sub>2</sub>O<sub>4</sub> CHẾ TẠO BẰNG PHƯƠNG PHÁP PHUN TĨNH ĐIỆN

**Nguyễn Văn Hoàng, Lê Minh Đức, Nguyễn Mạnh Hùng,  
Nguyễn Văn Duy, Nguyễn Đức Hòa, Nguyễn Văn Hiếu**

**Tóm tắt:** Trong nghiên cứu này, sợi nano ZnFe<sub>2</sub>O<sub>4</sub> được tổng hợp thành công bằng phương pháp phun tĩnh điện. Ảnh hiển vi điện tử quét phát xạ trường (FESEM) cho thấy hình thái đặc trưng của sợi nano chế tạo bằng phương pháp phun tĩnh điện có dạng như mạng nhện, đường kính sợi khoảng 30-100 nm và được cấu thành từ rất nhiều hạt nano. Phổ tán sắc năng lượng (EDX) chỉ ra rằng thành phần sợi nano ZnFe<sub>2</sub>O<sub>4</sub> gồm các nguyên tố Zn, Fe và O. Giảm đồ nhiễu xạ tia X (XRD) chứng minh cấu trúc mạng dạng lập phương của sợi thu được. Quan sát trên ảnh FESEM và tính toán kích thước hạt từ giảm đồ XRD cho thấy kích thước hạt nano tăng khi nhiệt độ ủ tăng. Hoạt năng cho quá trình phát triển hạt của sợi nano ZnFe<sub>2</sub>O<sub>4</sub> tính được vào khoảng 10 kJ/mol. Hoạt năng này khá nhỏ cho thấy hạt nano ZnFe<sub>2</sub>O<sub>4</sub> dễ dàng phát triển khi nung ở nhiệt độ cao.

**Từ khóa:** Hoạt năng; ZnFe<sub>2</sub>O<sub>4</sub>; sợi nano; phun tĩnh điện.

Received: 28/5/2021; Revised: 15/7/2021; Accepted for publication: 17/9/2021

